Aircraft de-icing using time-reversed guided waves

Thomas Clarke[*]
Federal University of Rio Grande do Sul (UFRGS), Porto Alegre, 91501-970, Brazil

Timothy Waters[†], Ian Stothers[‡]
Institute of Sound and Vibration Research, University of Southampton, Southampton, SO17 1BJ, UK

and
Davide Raffaele[§]
Department of Industrial Engineering, University of Trento, Trento, 38123, Italy

The passage of elastic waves in layered structures gives rise to interfacial stresses that can cause delamination. Whilst usually undesirable, this can be exploited to remove unwanted accretions from a substrate, such as ice from an aircraft wing. High amplitude transient waves, such as those induced by electro-expulsive de-icing systems, have proved effective, although their range is limited in part due to pulses spreading out with propagation distance from the actuator. In this paper, the phenomenon of wave dispersion which causes this effect is exploited through time reversality to focus waves both spatially and temporally and hence amplify the peak response at a chosen position. Harmonic finite element analysis is first undertaken to determine the wave bearing characteristics of a simplified representation of a wing leading edge. Transient analysis is then performed on the structure with an attached ice layer to focus disturbances of bandwidths up to 50 kHz at different chosen points. The amplitude of the peak shear stress between the ice and substrate is bandwidth dependent and predicted to be up to 30 times higher than due to a comparable pulse input. Predicted peak accelerations are successfully validated experimentally for a limited bandwidth of 10 kHz.

Keywords: guided waves, focussing, time reversal, transient vibration, ice removal

[*]Visiting Academic, University of Southampton/Associate Professor, UFRGS/Corresponding author: clarke@ufrgs.br
[†]Professor, University of Southampton
[‡]Visiting Academic, University of Southampton
[§]Graduate Student, University of Southampton / Research Fellow, University of Trento

I. Introduction

ICE removal from airplane wings during flight is essential for operational safety. Even thin layers of ice are sufficient to increase drag, reduce lift and cause excessive vibration due to airflow imbalances [1]. Most conventional de-icing technologies heat the wing to melt the attached ice, either using hot air bled from the engines or embedded thermoelectric heater elements [2]. Whilst effective and reliable, there are disadvantages to both approaches, most notably their high energy consumption and associated carbon footprint which has driven research into low energy alternatives. Of these, vibration and shock-based techniques are most prevalent in the literature. Vibration generates interfacial shear stresses between the wing substrate and the ice which can cause ice shedding if the bond strength is exceeded. The large amplitudes required have led some researchers to excite higher order structural resonances, at hundreds [3], [4] or thousands of Hertz [5]. Budinger et al. modelled stress generation at the adhesion interface of an iced plate for extensional and flexural modes in the range of 100 Hz to 100 kHz, concluding that flexural modes require less energy to initiate cohesive fractures, particularly at higher frequencies [6], [7]. Multiple modes are typically required that exhibit different stress nodal lines necessitating frequency sweeps or tracking of natural frequencies [8]. Alternatively, a wave approach can be adopted whereby interfacial stresses are induced by incident Lamb or shear horizontal waves excited by piezoelectric actuators at typically ultrasonic frequencies, without recourse to standing wave behaviour in the structure [9]. The actuator is usually driven maximally at resonance to provide a high enough input, which can cause debonding, cracking or excessive heating of the actuator itself [10], [11]. Some notable success has been demonstrated in removing ice from a substrate in both laboratory and wind tunnel tests [12], [13]. However, to the authors' knowledge, no continuous vibration-based ice protection system has been certified to date.

Shock based techniques remove ice by the same mechanical principle but via short, high amplitude transient response. Electroimpulsive de-icing (EIDI), which can be traced back to a patent filed in 1939 [14], discharges capacitors through inductive coils positioned on the wing leading edge. Labeas et al. used finite element modelling to predict the stress distribution at the interface between an aluminium wing leading edge and ice layer due to a 1 ms sinusoidal pulse delivered by electroimpulsive actuators. Forces of the order of 100 N were predicted to debond up to 98% of the accreted area depending on the ice thickness. Separate actuators were required for each wing bay. Electro-expulsive ice protection systems work on the same principle as EIDI but the impulsive excitation is induced by discharging capacitors through conductors in close proximity [15]. Cox and Co have developed an Electro-Mechanical

Expulsion Deicing System (EMEDS) which has been certified for some applications. The range from which any impulsive actuator can remove ice is inherently limited due to a combination of wave attenuation due to damping, wave scattering at joints and spreading out of the pulse as it propagates. The latter arises due to wave dispersion, i.e. that elastic waves in structures possess frequency dependent wave speeds.

Previous research by the authors has sought to compensate for and exploit wave dispersion to amplify the shock response at arbitrary points along the structure [16]. Initial work concerned the successful removal of an ice substitute from a beam [17], [18]. The up-chirp excitation signal gives slower, low frequency waves a 'head start' compared to faster, higher frequencies such that all frequency components arrive synchronously to produce a shock at a chosen focal point. The focal point can be moved by modification of the excitation signal in which the required time delays between frequency components are encoded. A practical limitation of this approach for aircraft de-icing is that prior knowledge of the dispersion relation is required, especially given likely time variance of the system due to ice accretion and other operational factors. The technique is also difficult to extend to structures in which multiple waves can propagate. A subsequent study by one of the authors [19] generalised this work to the case of a semi-cylindrical structure, chosen as a simple representation of a wing leading edge. Raffaele used time-reversality to derive an excitation waveform that can compensate for the dispersive behaviour of a plurality of wave modes responsible for propagation of the disturbance without prior knowledge of their dispersion relations. Modest increases in peak acceleration were observed as compared to time harmonic excitation at an optimally chosen frequency.

This paper aims to evaluate the conditions under which time-reversal focussing of vibrational waves is effective. The work considers the same semi-cylindrical structure but represents a significant extension to [19] in a number of respects: (i) an ice layer has been incorporated in a 3D finite element model of the waveguide enabling interfacial shear stresses to be simulated and hence the force required to remove ice to be estimated; (ii) the effect of bandwidth on peak response has been systematically investigated, and the benefit of ultrasonic frequencies quantified; (iii) a causal damping model has been included to quantify the effects of energy losses on peak response; and (iv) time reversal has been implemented experimentally, for a low bandwidth, which has produced results that are consistent with the model.

The paper is organised as follows. Section 2 presents a semi-analytical finite element model from which the number and dispersive behaviour of freely propagating waves can be established. The results are used to verify the dispersion curves obtained from forced analysis of a 3D finite element model. In section 3, a Rayleigh damping model

is adopted and the damping coefficients adjusted to match measured decay rates on a practical realisation of the structure. In Section 4 the finite element model is used to simulate frequency response functions which are subsequently used to compute the response to arbitrary transient inputs by frequency domain convolution. Input waveforms that produce shock response at different focal points are obtained by time reversal and the effects of bandwidth and damping on peak response are quantified. Finally, time reversal is implemented experimentally in section 5.

II. Free wave propagation

During flight, ice accumulates principally on the leading edge of lifting surfaces due to flow stagnation. The construction of leading edge structures varies significantly, particularly between fixed and rotary wing aircraft. This study focusses specifically on thin-walled, singly curved structures resemblant of erosion shields of fixed wing aircraft. A uniform, thin-walled half-cylinder of radius 100 mm was therefore chosen as a simplistic representation of a wing leading edge. The half-cylinder was attached to a 200 mm thick, flat backing plate, as shown in cross section by the mesh in Fig. 1. It is noted that this simplified geometry results in a one-dimensional waveguide which does not exhibit attenuation due to geometrical spreading or wave scattering due to stiffeners and other discontinuities.

First, dispersion relations are obtained for elastic waves propagating along its length. Whilst not explicitly required for implementation of the time reversal process, an assessment of their plurality, dispersiveness, excitability and sensitivity to ice accumulation is a useful precursor. Dispersion curves are initially presented from a semi-analytical finite element (SAFE) analysis of the structure. Comparable results are then obtained from a finite element model which, whilst less convenient for obtaining dispersion curves, is readily able to simulate forced responses due to arbitrary input waveforms.

A. Semi-analytical modelling

The semi-analytical finite element (SAFE) method is a convenient and computationally efficient technique for calculating the dispersion curves and mode shapes of freely propagating waves without complications arising due to reflections from terminations or choice of excitation. Spatial variation of the response is assumed to be harmonic in the direction of propagation such that only the 2D cross section is discretised. Elemental formulations differ from those in conventional FE analysis but SAFE analysis is available in some commercially available simulation software. The reader is referred to the literature for detailed explanations of the method, e.g. [20].

The mesh refinement was determined through a convergence study to establish an acceptable trade-off between numerical error and computation time. The model was run in COMSOL Multiphysics through an implementation of the necessary code in MATLAB. The waveguide cross-section is shown in Fig. 1; it consists of 2 mm-thick sheet aluminium attached rigidly to a 100 mm-wide, 10 mm-thick aluminium backing plate. This cross-section was automatically meshed with an instruction that 1 mm quadratic quadrilateral elements should be adopted, an element size that was defined through a mesh convergence study. The inclusion of an ice layer is essential in the forced analysis later to predict the stress distribution at the interface with the substrate. It is also included here in the free wave analysis to assess its likely effect on the dispersion curves. Whilst ice thickness is variable in practice a uniform 1 mm thick ice sheet tied to the whole of the curved plate was used for simplicity. The material properties used in all models are listed in Table 1, in which the chosen nominal values for ice are very similar to those reported for pure ice in [21].

Table 1. Material properties of aluminium and ice

	Aluminium	Ice
Density (kg/m^3)	2700	920
Young's modulus (GPa)	68.8	8.1
Poisson's ratio	0.33	0.35
Pressure wave velocity (m/s)	5048	2967
Shear wave velocity (m/s)	3095	1805

Fig. 2 shows the dispersion curves predicted by the models for propagating modes up to 50 kHz; more than 20 modes are apparent, most of which begin to propagate above their respective cut-off frequencies. The curves convey their dispersive nature, the gradients of which are related to group velocity. The presence of ice causes shifts to many of the curves, an effect that can be explained, for the lower order modes at least, by mass-loading of the structure.

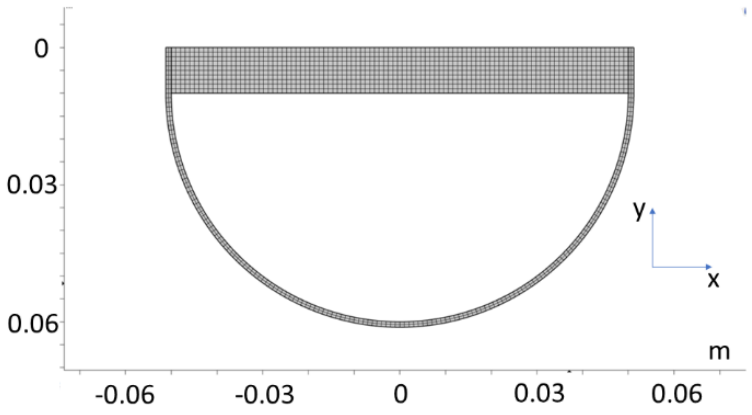

Fig. 1. Cross-section and SAFE mesh of the waveguide adopted as a representation of the leading edge of an airplane wing.

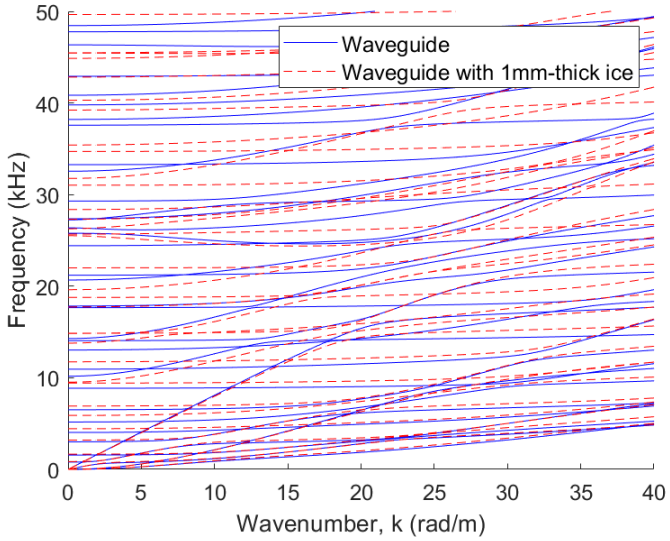

Fig. 2. Dispersion curves obtained from the SAFE model with and without a 1 mm ice layer.

B. Finite element modelling

A complete 3D finite element model of the wing structure was generated in ABAQUS. Its express purpose was to simulate forced wave propagation, although dispersion curves were first estimated and validated against the SAFE model. The cross-section dimensions were chosen to be the same as considered in Fig. 1. The model is 6 m in length, half of which consists of an absorptive region (built according to [22]) that minimises reflections from one end (see Fig. 3(b)). Fig. 3(a) shows the mesh considered for this model, its refinement having been established in a separate convergence study.

The mesh was optimised through a convergence study, and consisted of linear 25 mm-long hexahedrons with 1 mm quadrilateral faces for the curved sheet and 2.5 mm quadrilateral faces for the backing plate. A unit force excitation was introduced at the reflective end of the waveguide, normal to and on the leading edge of the curved surface. Harmonic solutions were obtained in steady-state for frequencies up to 50 kHz. As for the SAFE model, a second FE model was also produced with a 1 mm-thick ice layer tied to the curved plate. Nodal displacement, and element-integrated shear stress in the case of the model with the ice layer, were monitored in 1 mm steps along the waveguide up to the beginning of the absorptive region. This produced sets of frequency response functions (FRFs) of both displacement and shear stress with respect to force as functions of position. Dispersion curves were estimated by applying a 2D-FFT to the displacement field. Fig. 4a shows all the modes that were excited in the FE model by applying this force; it can be seen that low frequency modes are more easily excited under these boundary conditions than higher frequency modes.

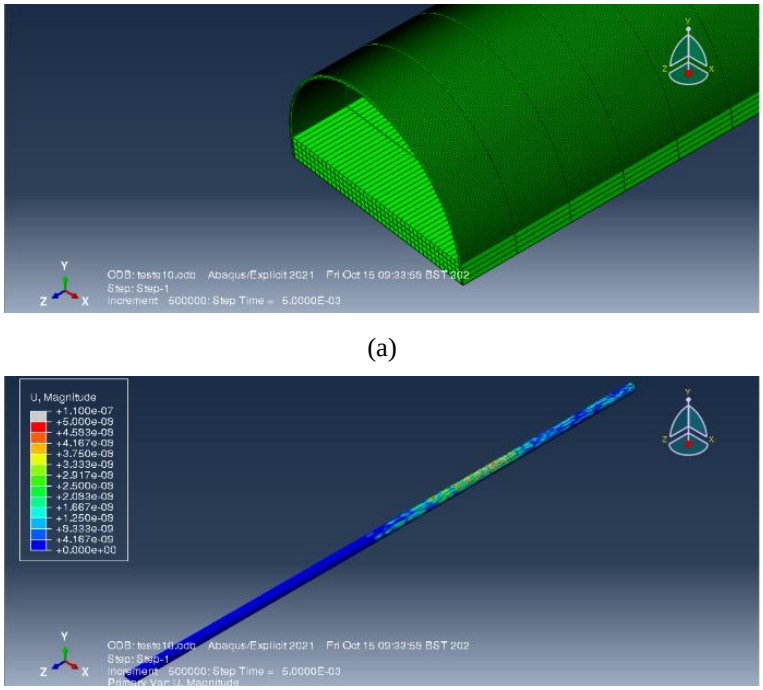

(a)

(b)

Fig. 3. (a) Detail of the 3D FEM waveguide cross-section; (b) Frame of a wide-band excitation pulse propagating along the waveguide (absorption region on the right).

C. Dispersion relations

Fig. 4b shows a comparison of the dispersion curves of the dominant modes in Fig. 4a (up to 10 kHz) from the SAFE and FE models when the ice layer is included. Some of the modes predicted by the SAFE model are absent from the 3D FE analysis results owing to the position and orientation of the input force and to the out-of-plane direction in which displacement in monitored along the waveguided. Hence, only dispersion curves that appeared in both models are included. There is a good match between the results of the two models, and the FE model is subsequently adopted for forced wave propagation calculations. Experimental validation of the dispersion curves up to 10 kHz, using the structure described later in section III, is presented in [19] but omitted here for brevity. The predominantly excited modes are in reasonably close agreement.

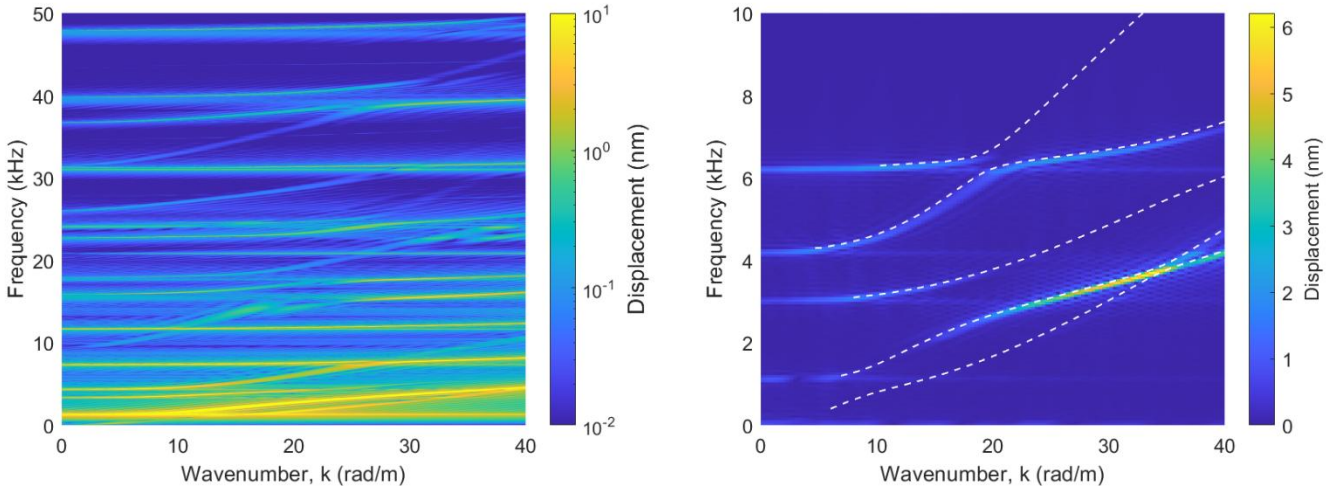

(a) (b)

Fig. 4: Dispersion curves up to (a) 50 kHz, and (b) 10 kHz with comparison between SAFE model (white lines) and 3D FE model (colour contours).

III. Damping and attenuation

In section 2, harmonic forced analysis of the FE model was performed to infer the free wave propagation behaviour of the waveguide. Structural damping was omitted for that purpose. However, damping is an important factor for time-reversal simulations reported in Section 4 for two reasons: firstly, the principle of time-reversality strictly holds only for conservative systems, and secondly, damping causes attenuation of wave amplitude with distance which counters the desired effect of wave focussing. In this section, a brief outline is provided for the damping model adopted and measurements on a laboratory structure are used to infer appropriate damping coefficients.

A. Damping model

A Rayleigh damping model was adopted to ensure causality in subsequent transient analyses. The propagation of a single positive-going wave in a one-dimensional waveguide can be written as:

$$\phi(x,t) = Ae^{\eta x}e^{i(\omega t - kx)} \quad (1)$$

where A is amplitude, x is propagation distance, *t* is time, ω is the circular frequency, *k* is the (positive) real part of the wavenumber, and η is the corresponding (negative) imaginary part. The Rayleigh damping model defines the latter as:

$$\eta = -k.\zeta \quad (2)$$

where the damping ratio ζ is given by [23]:

$$\zeta = \frac{1}{2}(\frac{\alpha}{\omega} + \beta\omega) \quad (3)$$

Attenuation in dB/m is given by -8.686 η.

Coefficients α and β pertain to mass and stiffness proportionality and control damping at low and high frequencies respectively. They can be selected by choosing a required damping ratio at two frequencies of interest and simultaneously solving equations of the form of Eq. (3). It is clear from Eq. (2) and (3) that the imaginary part of the wave number and hence attenuation are both mode and frequency dependent.

B. Attenuation

Fig. 5 shows an experimental realisation that closely resembles the FE models presented earlier. The curved shell is bonded to the backing plate which is expected to introduce significant damping. The structure is 3 m long of which about 40 cm of one end is buried in a box of sand of tapered thickness (not shown) to reduce reflections and the other end is free. A roving instrumented hammer (PCB model 086E80) and reference accelerometer (PCB model 352C22) were used to reciprocally measure 200 FRFs with a bandwidth of 10 kHz and a spacing of 0.01 m. The FRFs were processed according to a British Standard [24] to obtain attenuation estimates in one-third octave bands. The results,

shown in Fig. 6(a), suggest attenuation levels between 2.3 and 2.9 dB/m depending on the one-third octave band considered.

Rayleigh damping coefficient values of α=527.8 rad/s and 6.4×10^{-7} s/rad were selected manually and the corresponding attenuation rates were estimated from simulated transfer functions by applying the same British Standard as for the measurements. The simulated and measured attenuation rates are compared in Fig. 6. for the 2-8 kHz octave bands. The values from the model straddle their measured counterparts and are typically within 20%. The damping ratio from the model for the full frequency range up to 50 kHz is shown in Fig. 7. The model was adopted for all subsequent simulations for which damping was included, notwithstanding the increase in damping from 10 to 50 kHz beyond the available measured frequency range.

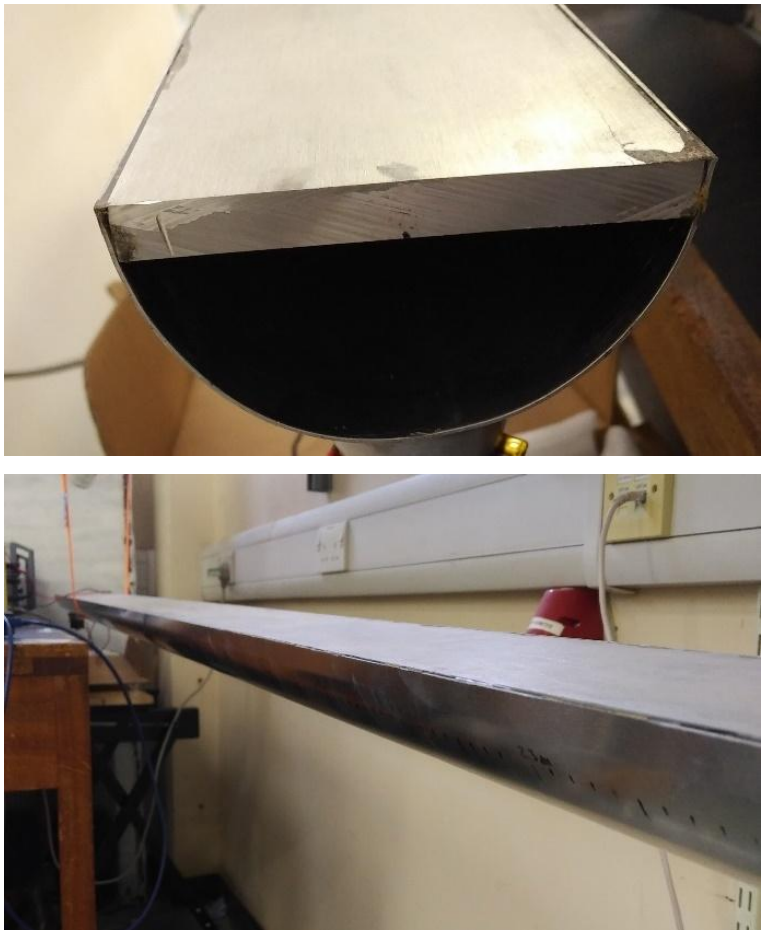

Fig. 5. Images of the waveguide used during experimental validation.

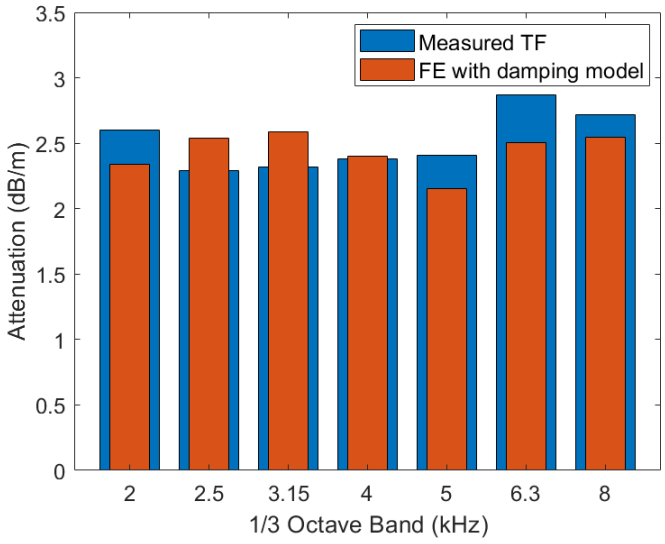

Fig. 6. Attenuation values obtained from measured (blue) and simulated (red) transfer functions. The simulated results were obtained using the damping ratio shown in Fig. 7.

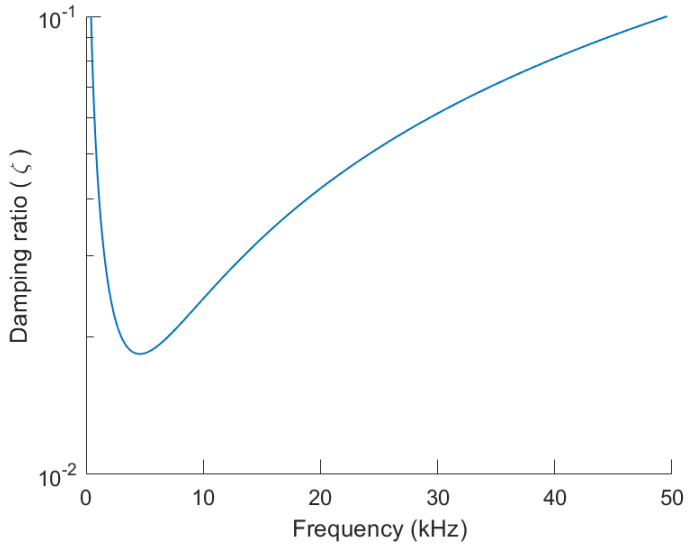

Fig. 7. Damping ratio as a function of frequency.

IV.Wave focusing

In this section, the FE model reported in Section 2 is deployed in a time reversal procedure [25] to simulate focussing of transient waves. The model includes a 1 mm thick, uniform ice layer. Initially, damping is omitted from the model and Rayleigh damping, as described in section 3, is introduced at a later stage. In the first step of the time reversal process, a pulse of desired bandwidth is set as the input waveform for a point force source applied at one end

of the waveguide and the response calculated at a chosen remote focal point. In the second step, the response is reversed in time and re-injected at the same excitation point. The disturbance compresses both temporally and spatially as it propagates towards the focal point.

An Ormsby wavelet was chosen as the input pulse for the first step and hence the desired waveform of the response in the second step owing to its flat spectrum over a controllable bandwidth [26]. The wavelet is defined by four frequencies: F1 and F3 control the bandwidth; F2 and F4 control the roll off rates, and the expression for the waveform is given by:

$$Ormsby(t) = \pi.\left(\frac{(F4.sinc(F4.t))^2-\left(F3.sinc(F3.t)\right)^2}{F4-F3} - \frac{(F2.sinc(F2.t))^2-(F1.sinc(F1.t))^2)}{F2-F1}\right) \quad (4)$$

This enabled the effects of bandwidth and hence crest factor on wave focussing to be investigated in a systematic and parametric fashion. In this study, F1 was varied from 0 kHz to 48 kHz and F3 was varied from 1 to 49 kHz, both in steps of 1 kHz. Parameters F2 and F4 were fixed at 1 kHz above F1 and F3 respectively.

In both steps of the time reversal process, the responses were calculated by convolution in time but computed in the frequency domain given FRFs of acceleration and shear stress with respect to force computed from harmonic solutions of the FE model. Thus, in the first step the response signal $a_1(x,t)$ and its spectrum $A_1(x,\omega)$ are given by

$$A_1(x,\omega) = H(x,\omega)F(\omega) \qquad a_1(x,t) = \mathcal{F}^{-1}\left(A_1(x,\omega)\right) \quad (5)$$

where $H(x,\omega)$ is the FRF of acceleration or shear stress at position x along the waveguide, $F(\omega)$ is the spectrum of the Ormsby wavelet and $\mathcal{F}^{-1}$ denotes the inverse Fourier transform. In the second step, the response signal $a_2(x,t)$ and its spectrum $A_2(x,\omega)$ are given by

$$A_2(x,\omega) = H(x,\omega)A_1^*(\omega) \qquad a_2(x,t) = \mathcal{F}^{-1}\left(A_2(x,\omega)\right) \quad (6)$$

where * denotes the complex conjugate. Conjugate symmetry was imposed on A_1 and A_2 to ensure real time responses.

Fig. 8 shows the input and response waveforms for one example case, when F1=1 kHz and F3=50 kHz. Fig. 8(a) shows the Ormsby wavelet for the first step of the time reversal process. Fig. 8(b) shows the waveform of the response at a focal point at 2 m which is time-reversed, see Fig. 8(c), and reinjected as the input for the second step to yield the response shown in Fig. 8(d). Fig. 8(c) also shows an alternative choice of input for the second step in which the input waveform is effectively digitised with one bit precision such that the signal is attributed a value of either 1 or -1 at each time sample [27] when amplitudes are above the rms value shown in Fig. 8b. The envelope of the input is rectangular thereby maximising the signal power whilst retaining phase information. In practice, it is necessary to set the signal to zero when it is below a threshold, chosen here as one-third of the rms of the signal. The initial disturbance is seen to arrive too early owing to energy being shifted to higher frequencies but the peak response is enlarged by a factor of nearly three in this case.

Fig. 9(a) shows a contour plot of peak acceleration per unit input as a function of bandwidth F1 to F3 at a focal point of 2 m. Fig. 9(b) shows the corresponding result for shear stress. The time-reversed input has not been 1-bit digitised until otherwise stated. The peak response generally increases with bandwidth, F3-F1, although frequencies below 10 kHz offer little improvement and can be marginally detrimental. Nonetheless, the complete bandwidth of 1-50 kHz is chosen for all subsequent results.

A maximal bandwidth of 1 to 50 kHz gives rise to stresses of nearly 0.1 MPa/N. The bond strength of ice to an aluminium substrate is dependent on many factors such as the type of ice and surface condition [28], [29]. However, Fig. 8(a) suggests that, subject to modelling assumptions, ice removal is possible with an input force of about 10 N peak if one adopts a reference value for bond strength of 1 MPa. This value is broadly representative of shear strength values of aluminium-ice interfaces according to the literature [30-33], which indicates values varying from 0.26 to 1.42 MPa depending on the type of ice formed, e.g. glaze or rime ice.

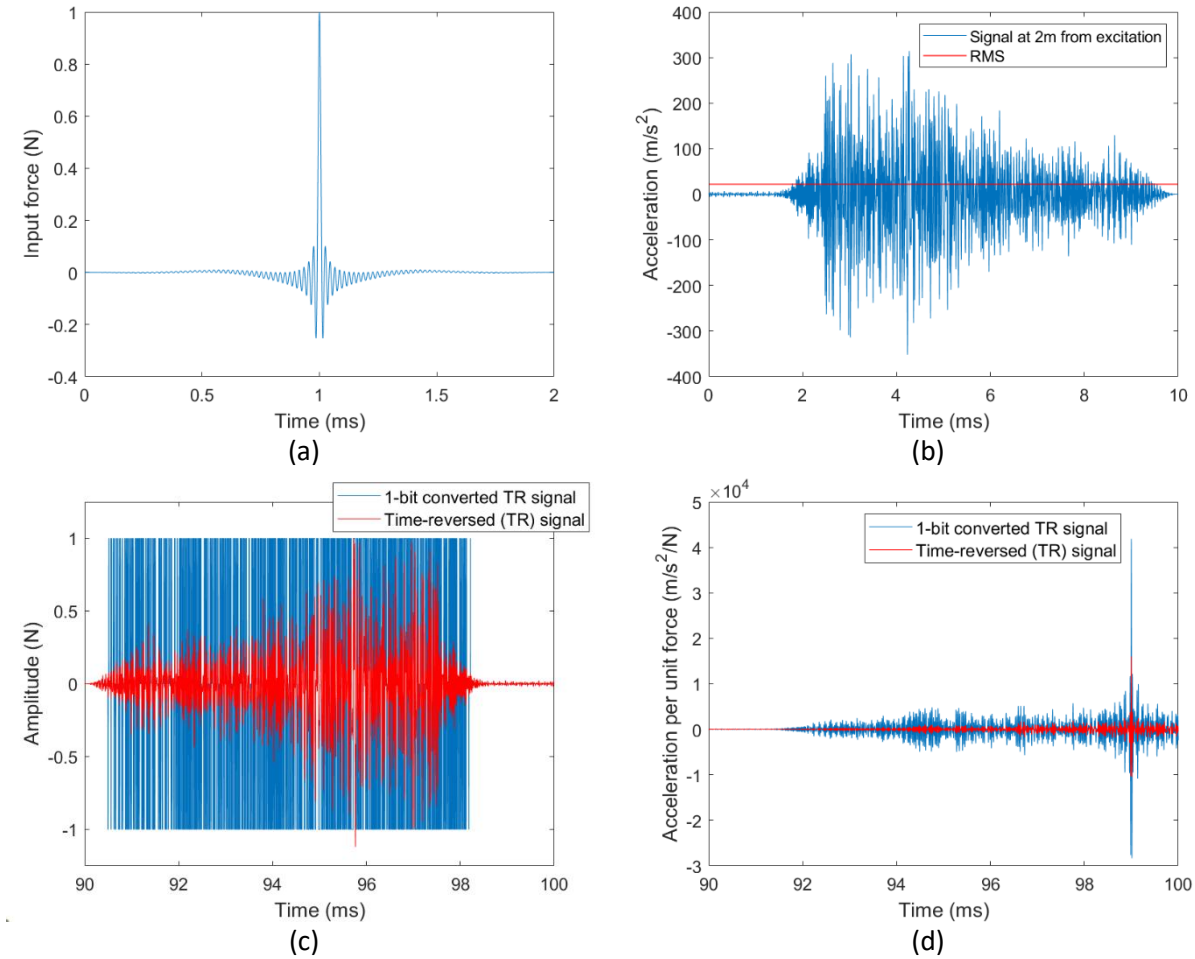

Fig. 8. Example signals: (a) Ormsby wavelet (1-50 kHz), (b) response at 2 m focal distance, (c) time-reversed and one-bit digitised waveforms, (d) response due to time-reversal.

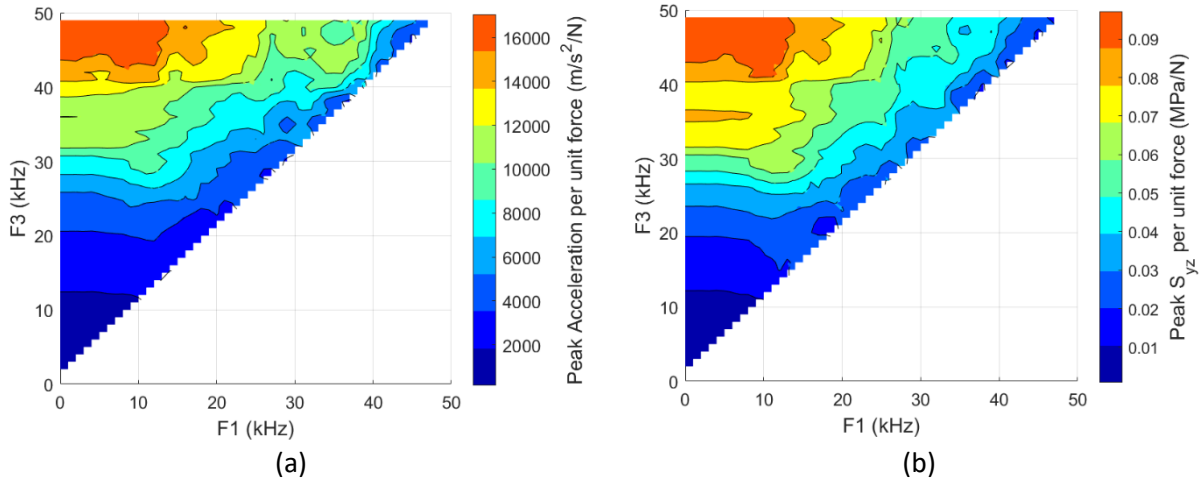

Fig. 9. Peak response per unit force input at 2 m from excitation without damping (a) acceleration and (b) shear stress.

Fig. 10(a) shows the peak stress as a function of propagation distance for a set of focal points from 0.5 m to 2 m. In each case the peak value occurs at the intended focal point, and the peak value generally increases with focal distance. The longer propagation time increases the duration of the excitation signal and hence more energy is input to the system. Also shown is the peak stress obtained in the first step of the time reversal process, i.e. when driven directly with an Ormsby pulse which disperses as it propagates along the waveguide. Time reversal is seen to provide a significantly larger peak stress than direct propagation of the original pulse. This is seen more clearly in Fig. 10(b) in which the peak stress from time reversal is normalised by that due to direct propagation of the pulse. Time reversality increases the peak response by a factor of 32 for a focal distance of 2 m.

Fig. 11 shows the peak acceleration as a function of propagation distance, both dimensional and normalised with respect to the case of direct propagation of the wavelet. The trends are similar to those for shear stress and a maximum gain of 35 is achieved at a focal distance of 2 m. The importance of acceleration as a response variable is restricted to its ease of measurement and hence model validation, as discussed in section 4.

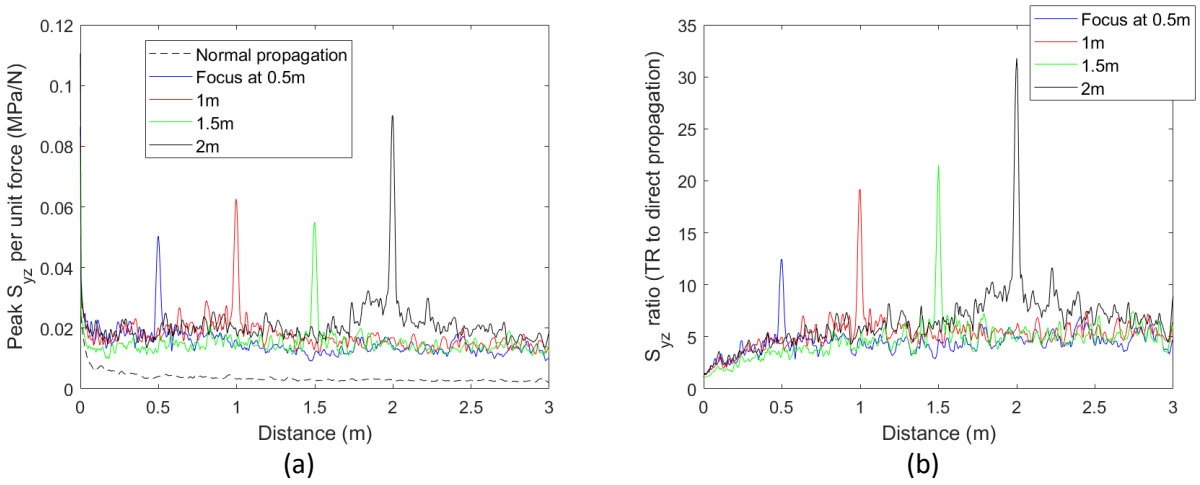

Fig. 10. Peak stress as a function of propagation distance achieved with time reversal (TR). (a) dimensional and (b) normalised by direct propagation.

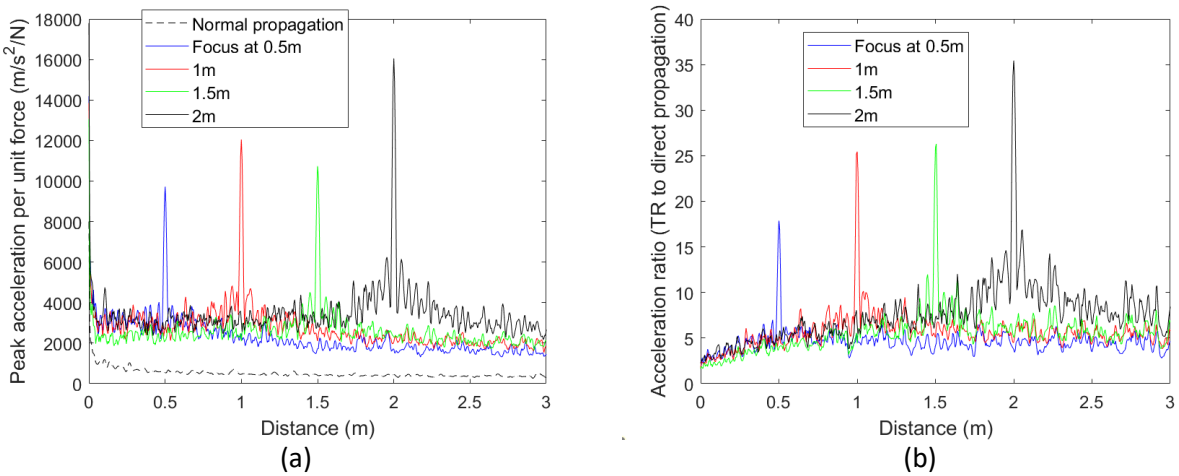

Fig. 11. Peak acceleration as a function of propagation distance achieved with time reversal (TR). (a) dimensional and (b) normalised by direct propagation.

Rayleigh damping is now included in the model, as discussed in Section 3, imposing 2% damping at 2 kHz and 8 kHz, as informed by measurements. Note that the proportionality to stiffness causes the damping to rise to 10% at 50 kHz which may not be representative of the real structure. Fig. 12 shows the peak stress as a function of propagation distance. As expected, damping has a detrimental effect on achievable values due to wave attenuation. In particular, the trend of increasing peak response with focal distance seen for the undamped system is reversed due to energy losses. Nonetheless, the peak stress achievable with time reversal is still at least 10 times higher than dispersed propagation of the wavelet.

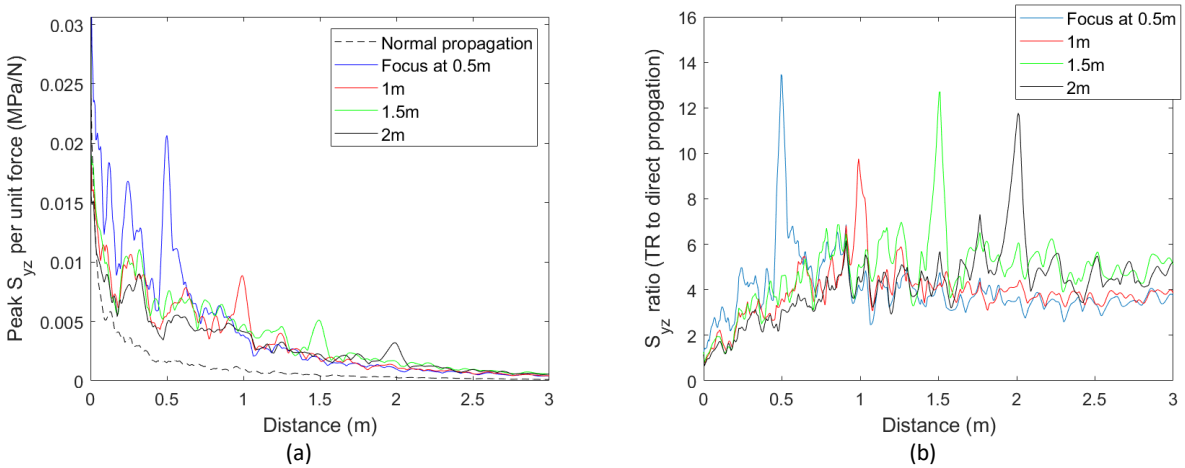

Fig. 12. Peak response per unit input force as a function of propagation distance (with damping). (a) shear stress and (b) normalised by direct propagation.

In all preceding results, the response at the intended focal point to an Ormsby wavelet has simply been time-reversed and re-injected at the same excitation position. The power of the input signal can be enhanced by manipulating its envelope in a number of ways, the most common being to apply one-bit digitisation. Fig. 13 shows the peak force required to induce a 1 MPa shear stress at the ice interface with and without one-bit digitisation. The reduction in required force achieved through one-bit digitisation depends on focal point and bandwidth but exceeds a factor of two in most cases. Fig. 13(b) suggests that ice may be removed at the closest focal point with a force of about 20-30 N and that the farthest focal point would require a force of about 90-100 N, provided that the bandwidth includes frequencies up to at least 30 kHz.

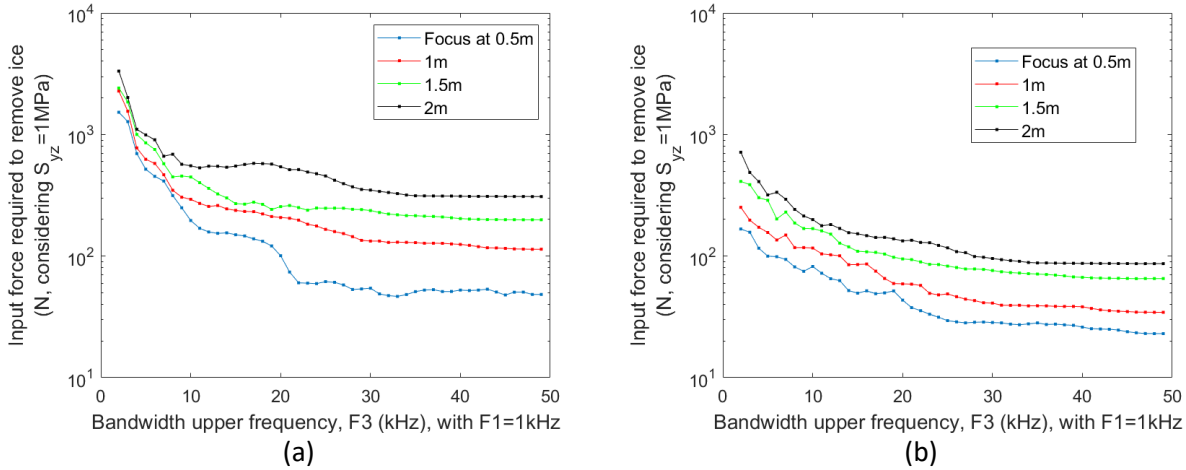

Fig. 13. Peak input force required to achieve a shear stress of 1 MPa with damping (a) without one-bit digitisation and (b) with one-bit digitisation.

V. Experimental implementation

Wave focussing was implemented experimentally on the 3 m long half-cylinder structure introduced in section 3. Conventional ultrasonic transducers were deemed unsuitable owing to their non-flat frequency response. Instead, a reduced bandwidth of 1-10 kHz was chosen for experimental validation purposes and an electrodynamic shaker (Data Physics, model V4) chosen which was known to have a reasonably flat frequency response in this frequency range [17]. The shaker was attached to the reflective end of the waveguide and the input force measured with a force gauge (PCB, model 208C01). The response at different positions along the waveguide was measured with a miniature accelerometer (PCB, model 352C22).

Fig. 14(a) shows the waveform and corresponding spectrum of the response 2 m from the shaker in the first step of the time reversal process, i.e. direct propagation of the disturbance. Here, the excitation signal was chosen to be a

1-50 kHz Ormsby wavelet, although the force input was strongly attenuated by the shaker above 10 kHz. In the second step, the signal was one-bit digitised and reinjected via the same shaker, resulting in the response signal and spectrum shown in Fig. 14(b). The gain of 1.6 afforded by the time reversal process is modest. However, this is in approximate agreement with the model for a bandwidth of 10 kHz, as shown in Fig. 15. A gain of 1.46 is predicted from 1-bit time reversal over a bandwidth of 1-10 kHz, whereas normal time reversal provides no benefit. Extending the bandwidth to 50 kHz increases the predicted gain on acceleration to up to six at this focal point.

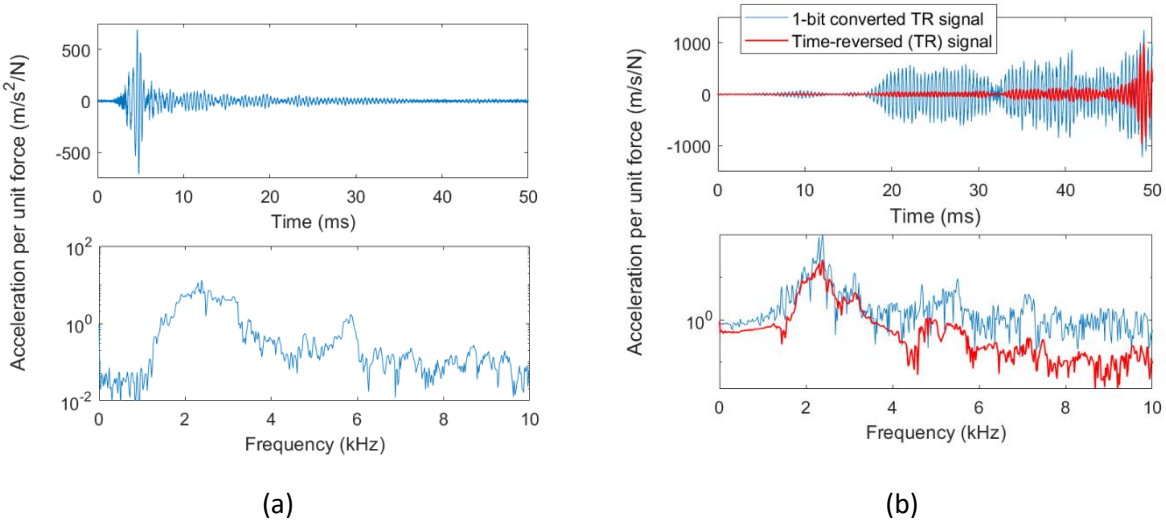

Fig. 14. Experimental signals and spectra (a) direct propagation signal at 2 m from excitation point; b) at 2 m using normal time-reversal and 1-bit time-reversal.

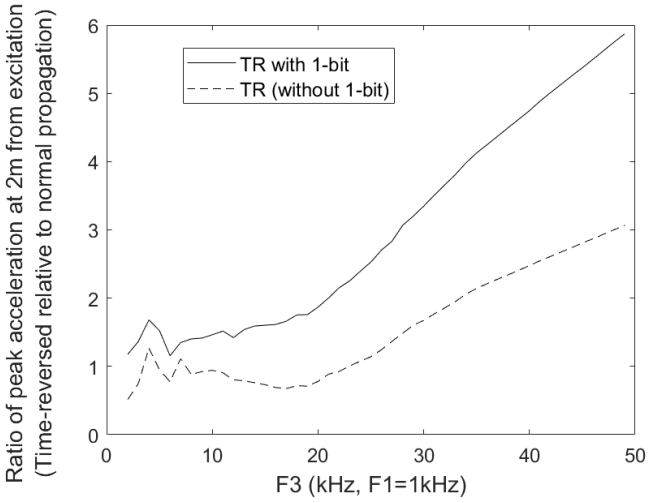

Fig. 15. Predicted gain in peak acceleration due to time reversal relative to the peak acceleration from direct propagation of the wavelet.

VI. Conclusions

This paper has assessed the feasibility of removing ice from a semi-cylindrical structure resembling a thin-walled wing leading edge by inducing impulsive responses. A finite element model has been developed to predict the transient response at any position along the structure to which a thin layer of ice is accreted. As expected, an impulsive disturbance spreads out and weakens as it is carried along the structure by a plurality of dispersive waves; this is detrimental to shock based de-icing technologies. The effects of dispersion have been countered here using time reversal focussing to derive a dispersed input waveform that gives rise to a shock response at any chosen remote position. The method is predicted to increase the peak shear stress at the ice-substrate interface by a factor of up to 30 in the absence of damping. Introducing a damping ratio that increases from 2% at 8 kHz to 10% at 50 kHz, peak forces of less than 100 N are predicted to induce peak shear stresses that exceed typical bond strengths of ice to aluminium. Whilst a bandwidth of 10-30 kHz is predicted to be most influential in maximising peak shear stress, experimental implementation has been reported for a reduced bandwidth of 1-10 kHz owing to the intrinsic limitations of electrodynamic shakers. A modest gain of about 1.6 is in line with predictions and provides partial validation of the model. A key objective of future work will be to couple an electromechanical model of a broadband ultrasonic actuator to the dynamic model of the structure and to validate it experimentally at ultrasonic frequencies.

This study has adopted a simplistic model of both the substrate and the ice layer to achieve qualitative insight into the potential performance benefits of wave focusing as compared to straightforward transient excitation. The finite element approach allows for more realistic wing structures to be investigated which may exhibit greater attenuation due to geometric spreading and wave scattering at joints. Extension from thin plate-like structures to solid rotor blades is a further avenue of research which can be explored using the same methodology as reported in this paper. In practice, ice accumulation is a complex thermomechanical process causing non-uniform thickness distributions and variable material properties. These issues would need to be modelled to provide quantitative performance predictions and validated through icing wind tunnel tests.

Funding Sources

The study reported in this paper was funded by Ultra Electronics PLC and is related to European Patent EP3630610.

Acknowledgments

The authors acknowledge the use of the IRIDIS High Performance Computing Facility, and associated support services at the University of Southampton, in the completion of this work.

References

[1] Civil Aviation Authority (2000). *Aircraft Icing Handbook.*

[2] Goraj, Z., "An overview of the deicing and anti-icing technologies with prospects for the future", *24th International Congress of the Aeronautical Sciences*, Yokohama, Japan, 2004.

[3] Struggl, S., Korak, J., Feyrer, C., "A basic approach for wing leading deicing by smart structures", *Conference on Sensors and Smart Structures Technologies for Civil, Mechanical, and Aerospace Systems*, 2011. https://doi.org/10.1117/12.880470

[4] Villeneuve, E., Volat, C., Ghinet, S., "Numerical and experimental investigation of the design of a piezoelectric de-icing system for small rotorcraft Part 1/3: Development of a flat plate numerical model with experimental validation", *Aerospace*, 7(5), 62, 2020. https://doi.org/10.3390/aerospace7050062

[5] Bai, T., Zhu, C.L., Miao, B., Li, K., Zhu, C.X. "Vibration de-icing method with piezoelectric actuators", *Journal of vibroengineering*, 17(1), pp. 61-73, 2015.

[6] Budinger, M., Pommier-Budinger, V., Reysset, A., Palanque, V., "Electromechanical resonant ice protection systems: energetic and power considerations", *AIAA Journal* 59(7), 2021. https://doi.org/10.2514/1.J060008

[7] Budinger, M., Pommier-Budinger, V., Napias, G., Costa de Silva, A., "Ultrasonic ice protection systems: analytical and numerical models for architecture tradeoff", *Journal of Aircraft*, 53(3), pp1-11, 2016. https://doi.org/10.2514/1.C033625

[8] Shi, Y., Jia, Y., "Multi-modal shear wave de-icing using fibre piezoelectric actuator on composite for aircraft wings", *IEEE/ASME Transactions on Mechatronics*, 20(10), 2018. https://doi.org/10.1109/TMECH.2018.2862433

[9] Kalkowski, M. Waters, T.P., Rustighi, E., "Delamination of surface accretions with structural waves: piezo-actuation and power requirements". *Journal of Intelligent Materials Systems and Structures*, 28 (11), 1454-1471, 2017. https://doi.org/10.1177/1045389X16672567

[10] Overmeyer, A., Palacios, J., Smith, E., "Ultrasonic de-icing bondline design and rotor ice testing", *AIAA Journal* 51(12):2965-2976, 2013. https://doi.org/10.2514/1.J052601

[11] Palacios, J., “A review of ultrasonic vibration for de-icing of aircraft”, *International Conference on Vibration and Vibro-acoustics*, 2014.

[12] Palacios, J., Smith, E, Rose, J., Royer, R., “Instantaneous de-icing of freezer ice via ultrasonic actuation,” *AIAA Journal*, Volume 49, Number 6, pp. 1158-1067, 2011. https://doi.org/10.2514/1.J050143

[13] Palacios, J., Smith, E, Rose, J., Royer, R., “Ultrasonic de-icing of wind tunnel impact icing,” *Journal of Aircraft* Volume 48, Number 3, pp 1020-1027, 2011. https://doi.org/10.2514/1.C031201

[14] Goldschmidt, R., British Patent Specification No. 505,433, 1939.

[15] Haslim, L.A., Lee, R.D., “Electro-expulsive separation system”, US patent 4,690,353, 1987.

[16] Waters, T.P., Stothers, I.M., “Ice protection system”, PCT/GB2018/051474, 2018.

[17] Waters, T.P., “A chirp excitation for focussing flexural waves”, *Journal of Sound and Vibration*, 439, 113-128, 2019. https://doi.org/10.1016/j.jsv.2018.07.028

[18] Waters, T.P., Harris, V, Mulchandani, H, Stothers, I.M., “Focussing flexural waves for accretion removal from a beam”, *International Conference on Noise & Vibration Engineering (ISMA*), Leuven, Belgium. 17 - 19 Sep 2018.

[19] Raffaele, D., “Focussing elastic waves in wing leading edge structures”. University of Southampton, Doctoral Thesis, 2022.

[20] Predoi, M.V., Castaings, M., Hosten, B., Bacon, C., “Wave propagation along transversely periodic structures”, *The Journal of the Acoustical Society of America*, 121 (4), 1935-1944, 2007. https://doi.org/10.1121/1.2534256

[21]. Palanque, E. Villeneuve, M. Budinger, V. Pommier-Budinger, G. Momen, Experimental measurement and expression of atmospheric ice Young's modulus according to its density, Cold Regions Science and Technology, Vol. 212, 2023, 103890. https://doi.org/10.1016/j.coldregions.2023.103890.

[22] Drozdz, M., Moreau, L., Castaings, M., Lowe, M.J.S., Cawley, P., Efficient numerical modelling of absorbing regions for boundaries of guided waves problems, *AIP Conference Proceedings*, 820, 126-133, 2006. https://doi.org/10.1063/1.2184520

[23] Luo, W., Rose, J.L., “Phased array focusing with guided waves in a viscoelastic coated hollow cylinder”, *The Journal of the Acoustical Society of America*, 121, 1945–1955, 2007. https://doi.org/10.1121/1.2711145

[24] British Standard. EN 15461:2008+A1:2010 - Railway applications. Noise emission. Characterisation of the dynamic properties of track selections for pass by noise measurements. British Standard Institution, 2010.

[25] Fink, M., “Time reversed acoustics”, *Physics Today*, Vol. 50, No. 3, pp. 34-40, 1997. https://doi.org/10.1088/0034-4885/63/12/202

[26] Ryan, H., Ricker, Ormsby, Klander, Butterworth – A choice of wavelets, *Canadian Society of Exploration Geophysicists Recorder*, 19(7), 1994.

[27] Montaldo, G., Roux, P., Derode, A., Negreira, C. and Fink, M. “Generation of very high pressure pulses with 1-bit time reversal in a solid waveguide”, *The Journal of the Acoustical Society of America*, 110, 2849–2857, 2001. https://doi.org/10.1121/1.1413753

[28] Raraty, L.E., Tabor, D., “The adhesion and strength properties of ice”, *Proceedings of the Royal Society A*, 245(1241), 1957. https://doi.org/10.1098/rspa.1958.0076

[29] Laforte, C., Laforte, J., “Deicing strains and stresses of ice substrates”, *Journal of Adhesion Science and Technology* 26, 603-620, 2012. https://doi.org/10.1163/016942411X574790

[30] Loughborough, D.L., Hass, E.G., “Reduction of adhesion of ice to de-icer surfaces”, *Journal of Aeronautical Sciences*, 13(3), 126-134, 1946. https://doi.org/10.2514/8.11328

[31] Stallbrass, J.R., Price, R.D., “On the adhesion of ice to various materials”, *Canadian Aeronautics and space Journal*, 199-204, 1963.

[32] Chu, M.C., Scavuzzo, R.J., “Adhesive shear strength of impact ice”, *AIAA Journal* 29, 1921-1926, 1991. https://doi.org/10.2514/3.10819

[33] Hassan, M.F., Lim, S.P., Lee, H.P., “The variation of ice adhesion strength with substrate surface roughness”, *Measurement Science & Technology* 21, 2010. https://doi.org/10.1088/0957-0233/21/7/075701